Int. J. Nano Dimens., 12 (2): 113-127, Spring 2021

ORIGINAL ARTICLE

Preparation, characterization and photocatalytic performance of nano α-Fe_2O_3 supported on metal organic framework of Cd(II) for decomposition of Cefalexin aqueous solutions

*Seyed Kamal Blourfrosh, Kazem Mahanpoor**

Department of Chemistry, Arak Branch, Islamic Azad University, Arak, Iran

Received 21 September 2020; revised 11 December 2020; accepted 16 December 2020; available online 28 December 2020

Abstract

In this study, a new and effective catalyst was prepared by supporting the α-Fe_2O_3 nanoparticles on a metal-organic framework (MOF). The synthesis of nano α-Fe2O3 photocatalyst was performed according to the reflux condensation method. The MOF was synthesized using cadmium nitrate and terephthalic acid. The nano α-Fe_2O_3 stabilized on the MOF by the solid-state distribution method. The α-Fe_2O_3/MOF was characterized by FTIR, XRD, SEM, EDX, TEM, N_2 adsorption-desorption, and TGA techniques. The α-Fe_2O_3/MOF was used as a catalyst to the UV/H_2O_2 photocatalytic decomposition of Cefalexin (CFX) in the aqueous solutions. This process was optimized and modelled using the full factorial experimental design. Initial concentrations of CFX, pH, α- Fe_2O_3/MOF amounts, and initial concentration of H_2O_2 were the variables for determining the optimal conditions and mathematical model. The highest decomposition percentage of CFX was 95.84%. The kinetics of this reaction was obtained pseudo-first-order at a constant rate of 0.0769 min^{-1}.

Keywords: *α-Fe_2O_3; Cefalexin; Metal-Organic Framework; Photocatalyst; Solid-State Distribution.*

How to cite this article

Blourfrosh S.K., Mahanpoor K. Preparation, characterization and photocatalytic performance of nano α-Fe_2O_3 supported on metal organic framework of Cd(II) for decomposition of Cefalexin aqueous solutions. Int. J. Nano Dimens., 2021; 12(2): 113-127.

INTRODUCTION

Drug compounds are a group of relatively new environmental risk factors. Antibiotics are a class of drugs that are usually present in small amounts in the environment. They can make pathogenic bacteria resistant to antibiotics [1]. Cephalosporins are the most common antibiotics that dissolve in water at different temperatures and pH ranges and can contaminate water [1]. Cephalexin (CFX) is an example of the antibiotic cephalosporin, which is used to treat bacterial infections such as pneumonia and other infections of the chest, skin, urinary tract, ears, and sometimes dental infections. The 250 mg to a maximum of 1 g of the drug is taken orally every 6 hours (cefalexin 250 or 500 capsules). The dose of cefalexin in children is 6 to 12 mg per kg of the child weight every 6 hours (oral suspension of cefalexin) [1].

Various methods were used for antibiotic removal of water sources, including adsorption, ion exchange, reverse osmosis, advanced oxidation and biological treatment. These methods have limitations. For example, antibiotics kill the microorganisms used in the biological treatment process, so these methods are not effective in removing antibiotic contaminants from the water. [2, 3]. Among the existing methods, photocatalytic methods are very effective for the treatment of wastewater containing antibiotic compounds [2, 3]. For example, the decomposition of amoxicillin was performed using direct UV irradiation and UV/H_2O_2 methods. The results of this study showed that 99% of primary amoxicillin was degraded by UV/H_2O_2 oxidation after 80 minutes [4]. Removal of the tetracycline antibiotic using the photocatalytic method under ultraviolet radiation has been reported. According to this report, 73% of tetracycline was eliminated after 300 min irradiations [5].

* Corresponding Author Email: *k-mahanpoor@iau-arak.ac.ir*

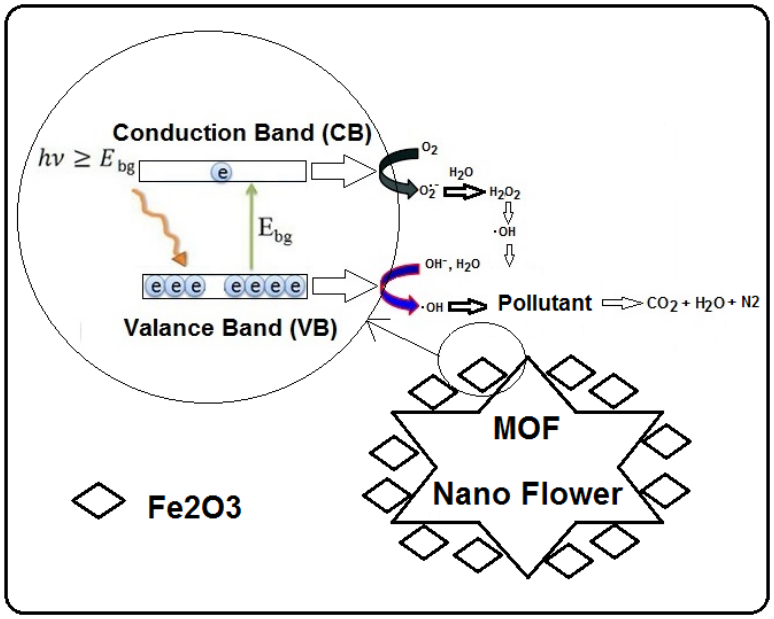

Fig. 1. Schematic of general photocatalyst reaction mechanism.

The catalyst is the most important factor in increasing the efficiency of the pollutant decomposition in the photocatalytic process. The α-Fe_2O_3, as a semiconductor with a 2.2 eV bandgap and high chemical stability is suitable for photocatalyst application, but its separation from water is difficult and costly [6, 7]. Stabilizing the catalyst on a suitable base is a suitable way to solve this problem. One group of compounds that can be used as a catalyst base are metal-organic frameworks (MOF) [8]. MOFs are composed of metal ions (clusters (attached to rigid organic molecules(connectors). These multiple connections create one, two, and three-dimensional, or porous, structures. The choice of the appropriate metal and bonder(connector) mainly affects the structure and properties of MOF. High design capability, regularity, flexibility and dynamics are key features of MOFs [9]. MOFs based on Cd (II) metal nodes with O-donor organic ligands such as rigid carboxylate ligands have thermal and chemical stability, structural variability, and luminescence properties [10]. The Cd-MOFs are insoluble in water, so the cadmium in their structure does not enter the water and therefore does not contaminate the water [10]. In this study, cadmium ions as a cluster and terephthalic acid as a connector were used to prepare MOF.

One of the most important features of semiconductors, including the α-Fe_2O_3, is that they have separate electron bands with two different energy levels in the last electron layer. The energy level of the valence band (VB) is lower than the energy level of the conduction band(CB). The energy gap between the valence and conduction bands is a feature of semiconductors, and its value depends on the nature of semiconductor material [7, 11].

When a photon of suitable energy (equal to or greater than the α-Fe_2O_3 band distance) strikes the α-Fe_2O_3 semiconductor, an electron is excited from the capacitance band to the conduction band. Because of this electron transfer, a positive hole is produced in the valence band and an extra electron in the conduction band, and then oxidation reactions occur in these electron-hole pairs and hydroxyl radicals.

If the catalyst base has adsorption properties, it can adsorb pollutant molecules to its surface. Because these molecules are in the vicinity of the photocatalyst, they will react with the active radicals produced by the catalyst and decompose rapidly. In this study, the α-Fe_2O_3 photocatalyst was fixed on the MOF adsorbent. A schematic of the photocatalyst mechanism is shown in Fig. 1 [7, 11].

The experimental design methods are used

in experiments that examine the effect of more than one factor on the response. One of the most important methods of experiment design is the full factorial method. In this experimental design, all levels of variables are compared with each other. Also, the effects of each factor level in the response based on other levels of factors are determined. Therefore, the effect of all variables can be evaluated by the full factorial method [12].

In this research, nano α-Fe_2O_3/MOF photocatalyst was prepared and identified with the appropriate techniques such as FT-IR, SEM, EDX, TEM, XRD, N_2 adsorption-desorption and TGA. The nano α-Fe_2O_3/MOF photocatalyst and H_2O_2 was used for photocatalytic decomposition of cefalexin in the batch photo-reactor. The optimum condition and the mathematical modelling of this process were performed by full factorial design.

EXPERIMENTAL

Materials

All chemicals including cadmium nitrate tetrahydrate, terephthalic acid, iron (III) chloride hexahydrate, urea, ammonia, hydrogen peroxide (30% purity), hydrochloric acid (37% purity), sulfuric acid (96% purity), sodium hydroxide, and ethanol were purchased from Merck company and were used without further purification. The required cefalexin (CFX) was purchased from Alborz Darou Pharmaceutical company (Qazvin, Iran).

Preparation of α-Fe_2O_3

The synthesis of the α-Fe_2O_3 photocatalyst was carried out according to the reflux density method of Bharathi *et al*. [11]. 4.054 g iron (III) chloride hexahydrate was dissolved in 50 ml deionized water. The urea solution (100 ml, 1 M) was added to this solution and was refluxed at the temperature of 95 °C for 12 hours. The sediment was separated by the centrifuge method. The precipitate dried in an oven at the temperature of 80 °C and it was put in a furnace at the temperature of 300 °C for 4 hours. The resulted red solid compound was cooled and rubbed in a mortar. In the following, the α-Fe_2O_3 photocatalyst synthesis reactions (1-5) are presented [11].

$$(NH_2)_2CO + H_2O \rightarrow 2NH_3 + CO_2 \quad (1)$$

$$NH_3 + H_2O \rightarrow NH_4^+ + OH^- \quad (2)$$

$$Fe^{3+} + 3OH^- \rightarrow Fe(OH)_3 \quad (3)$$

$$Fe(OH)_3 \leftrightarrow FeOOH + H_2O \quad (4)$$

$$2FeOOH \xrightarrow{300℃} \alpha\text{-}Fe_2O_3 + H_2O \quad (5)$$

Synthesis of MOF

Tetra hydrates cadmium nitrate (6.169 g) was dissolved in 50 ml deionized water, terephthalic acid (2.491 g) was dissolved in 50 ml of deionized water and ethanol solution (50% v/v). These solutions were mixed and then stirred for half an hour. The resulting solution was placed in an autoclave at 120 °C for 15 hours. The product was cooled to ambient temperature, and the crystals were separated by centrifugation. The crystals were washed by deionized water several times and dried in an oven at the temperature of 90 °C.

Stabilization of α-Fe_2O_3 on MOF

The α-Fe_2O_3 was stabilized on the MOF using the solid-state dispersion (SSD) method [13]. In this method, α-Fe_2O_3 (1 g) was mixed with MOF (3 g) using ethanol (5 ml) by an agate pestle and mortar; the ethanol was evaporated. The mixture was dried at 110 °C and placed in the furnace at 400 °C for 5 hours.

Apparatus

Furnace (Sef-201 Korea), oven (OF-02), and ALC4232 centrifuge have been used to make the catalyst. XRF model (Nitin XL 3t), XRD model (DX-27Mini 40kV/25mA), SEM model (Philips XL-30), TEM model (Philips EM208S) and FT-IR model (Perkin Elmer Spectrum 400) devices have been used to identification of the catalyst. N_2 adsorption/desorption isotherms at 77 K were measured using volumetric adsorption equipment (Bedsore-Max-S, BEL Japan Inc., Japan). The TGA device (Perkin Elmer Pyres 1, USA) was used to determine the stability and thermal degradation properties of the samples. Chemical oxygen demands (COD) of samples were measured by the potassium dichromate titration method (Standard Method 5220). All Ultraviolet/Visible (UV/Vis) absorption spectra for determining COD was obtained by an Agilent 8453 spectrophotometer. Total organic carbon (TOC) of samples was measured by ANATOC ™ Series II manufactured by the Australian SGE Company.

A 500 ml Pyrex reactor was put inside the wooden cube of side size of 60 cm. Three Phillips UV lamps (15 watts) are installed in the upper part of the wooden cube. The liquid inside the reactor

Table 1. Range and level of variables.

Variables	Range		
	-1	0	+1
CFX initial con. (ppm)	40	70	100
Catalyst amount. (mg. L^{-1})	50	100	150
H_2O_2 initial con. (ppm)	5	10	15
pH	4	7	10

Table 2. Experiment design of CFX decomposition by full factorial method.

Test No.	Catalyst amount. (mg. l^{-1})	CFX initial Con. (ppm)	H_2O_2 initial Con. (ppm)	pH	Decomposition percentile (%)
1	-1	+1	-1	-1	59.70
2	+1	+1	+1	+1	64.20
3	+1	-1	+1	-1	95.84
4	+1	+1	-1	-1	62.54
5	-1	+1	+1	-1	52.32
6	+1	-1	-1	+1	75.27
7	+1	-1	-1	-1	90.74
8	+1	+1	-1	+1	47.07
9	0	0	0	0	69.40
10	+1	+1	+1	-1	69.18
11	-1	-1	+1	-1	69.50
12	0	0	0	0	69.38
13	-1	-1	-1	+1	71.18
14	-1	+1	-1	+1	52.60
15	-1	+1	+1	+1	56.22
16	0	0	0	0	69.16
17	-1	-1	-1	-1	77.67
18	-1	-1	+1	+1	74.10
19	+1	-1	+1	+1	92.02

was continuously mixed with a magnetic stirrer. A fan was placed behind the cube to ventilate the air inside the box.

Procedure of photocatalytic decomposition of CFX

The full factorial designs method with the different variables containing initial concentrations of CFX, α-Fe_2O_3/MOF amounts, initial concentration of H_2O_2 and pH (as specified in Table 1 and 2) was used for optimization and process modelling.

Sulfuric acid and sodium hydroxide solutions (0.1 mol. l^{-1}) were used to adjust pH. For the photocatalytic decomposition of CFX, a solution containing the known concentration of CFX and photocatalyst (according to Table 2) was prepared and allowed to equilibrate in the dark for 30 min (to eliminate absorption effects). Then a certain amount of hydrogen peroxide was added, and the sample was exposed to ultraviolet radiation. UV-Vis spectrophotometric method was used to measuring the CFX concentration. The maximum wavelength of the CFX aqueous solution was 260 nm.

RESULTS AND DISCUSSION

Identification of Catalyst

The photocatalyst was identified with XRD, SEM, EDX, TGA, N_2 adsorption-desorption and FTIR techniques. The FTIR spectrum was used for the identification of the functional groups of the synthesized compounds. In the FTIR spectrum of α-Fe_2O_3 (Fig. 2-a), OH stretching and bending mode are specified from 1620.10 to 3415.12 cm^{-1}. The Fe-O adsorption peak was identified from 477.39 to 567.32 cm^{-1} [14]; Weak peaks of 1085.67 and 2344.99 cm^{-1} were respectively detected for the C-O and N-H bands in urea molecules, which did not react and were adsorbed on iron oxide [14, 15]. In the FTIR spectrum of MOF (Fig. 2-b), absorption peaks at 3416.54 cm^{-1} were recognized

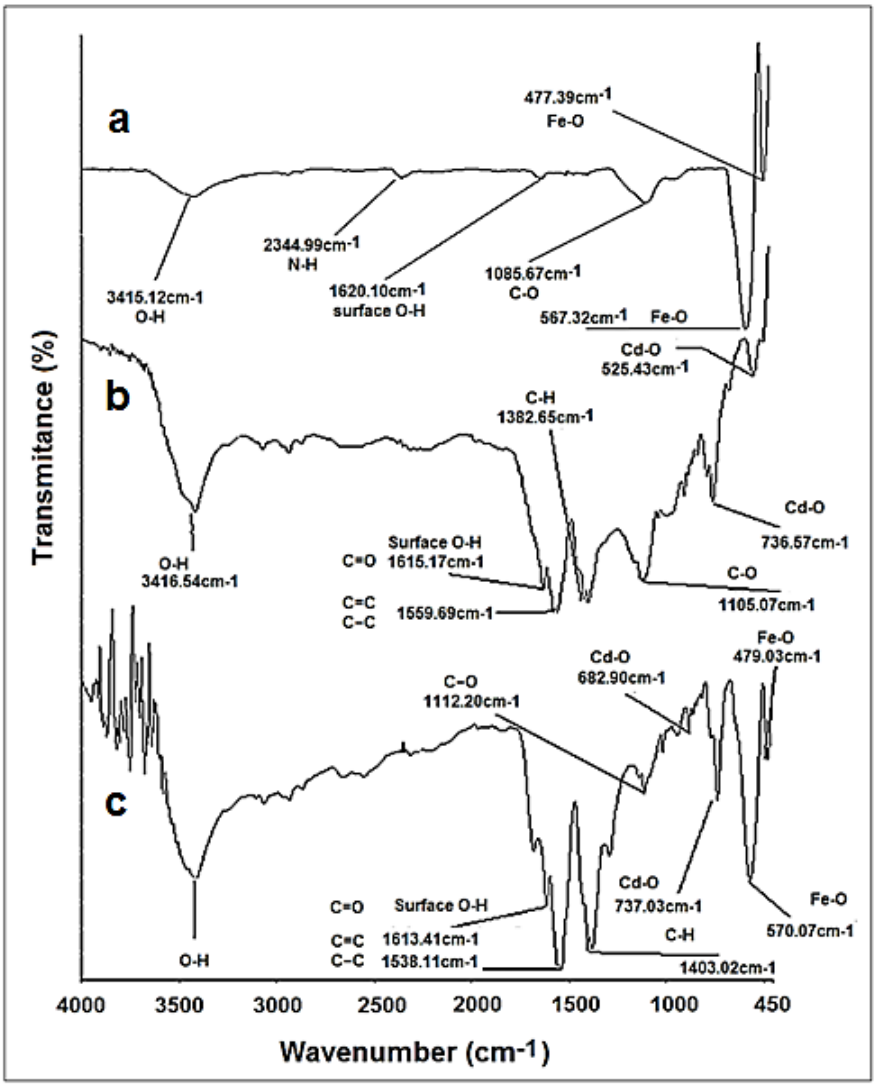

Fig. 2. FTIR spectroscopy of $_{\alpha}$-Fe_2O_3 (a), MOF (b) and α-Fe_2O_3/MOF(c).

to the O-H stretching mode. The absorption peaks of 1559.69 and 1615.17 cm^{-1} in the resonance structure of the benzene ring are attributed to C = C and C-C bonds, and these peaks also belong to the C = O bonds of the carboxylic acid groups in the terephthalic acid structure. Absorption peaks of 1382 and 1105 cm^{-1} are related to C-H bonds in the Benzene ring and C-O bond in a carboxylic acid; absorption peaks of 525.43 and 736.57 cm^{-1} are related to Cd-O bonds [16]. In the α-Fe_2O_3/MOF spectrum (Fig. 2-c), there are all absorption peaks observed in the MOF spectrum with a minor shift.

Fig. 3 presents the XRD patterns of pure α-Fe_2O_3 (Fig. 3-a) and MOF (Fig. 3-b) and α-Fe_2O_3/MOF (Fig. 3-c). As shown in the XRD patterns, the phase composition and crystallization of the α-Fe_2O_3 and MOF has not changed after the stabilization process [11, 15]. The average size of the α-Fe_2O_3 nanoparticles supported on the MOF has obtained 82.7 nm by applying the Debye Scherrer equation [17].

Fig. (4-a_1) presents the scanning electron microscope (SEM) images of the synthesized MOF that have porous and flower-like structures like to Dahlia. The particle size distribution diagram of MOF (Fig. (4-a_2)) shows that about 30% of the particles have dimensions of 25 to 35 nanometers. Fig.(4-a_3) shows the TEM imaging on the surface morphology of MOF-flowers that is of the multi-layered structure, where wrinkled MOF nanosheets were stacked into different directions

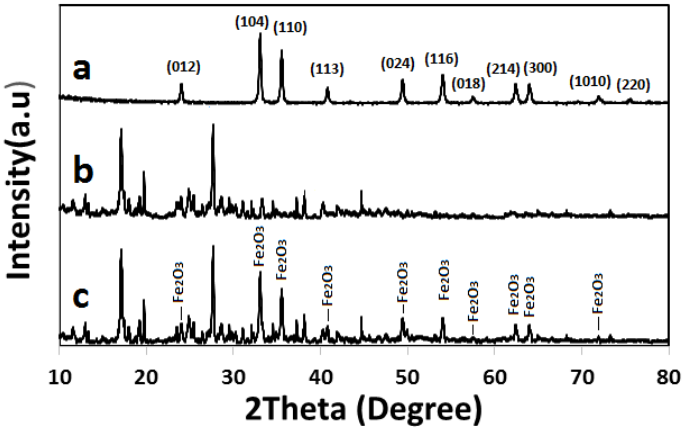

Fig. 3. XRD pattern of α-Fe_2O_3 (a), MOF (b)and α-Fe_2O_3/MOF(c).

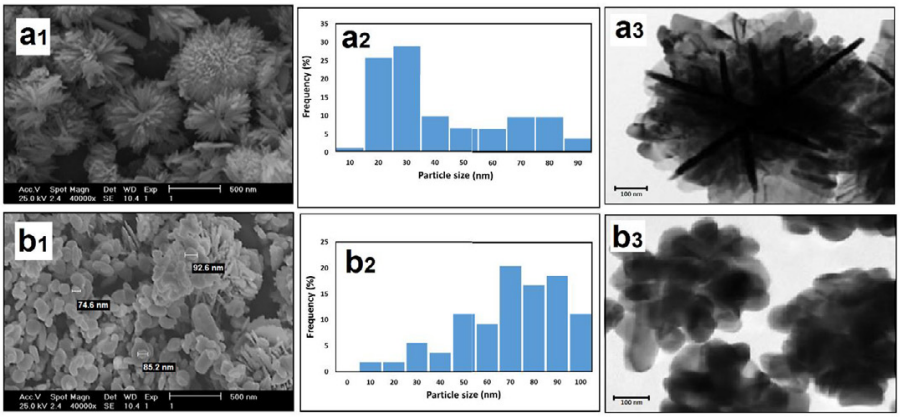

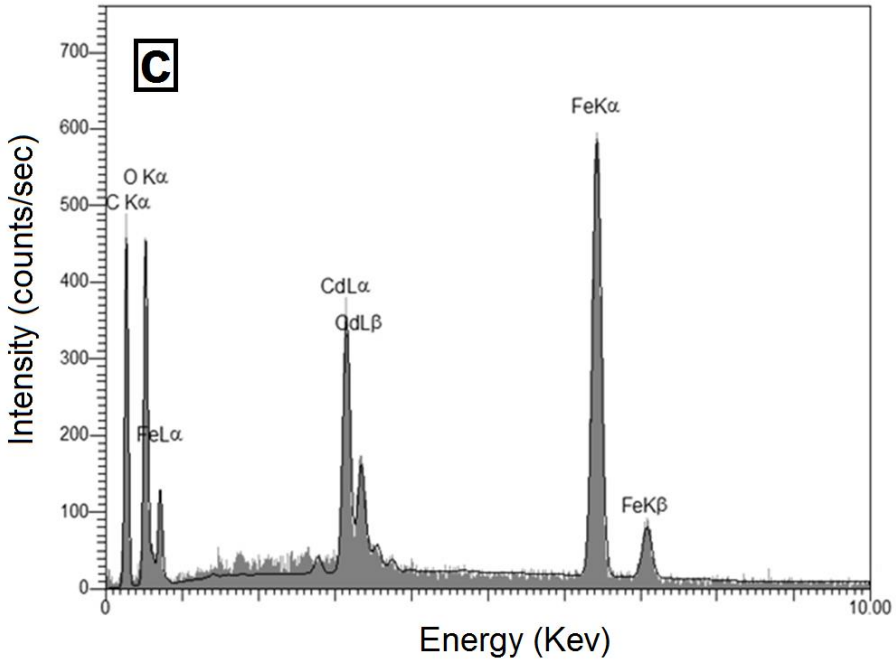

Fig. 4. SEM image of MOF (a_1) and α-Fe_2O_3/MOF (b_1), particle size of MOF (a_2) and α-Fe_2O_3/MOF (b_2), TEM image of MOF (a_3) and α-Fe_2O_3/MOF(b_3), and EDX of α-Fe_2O_3 /MOF(c).

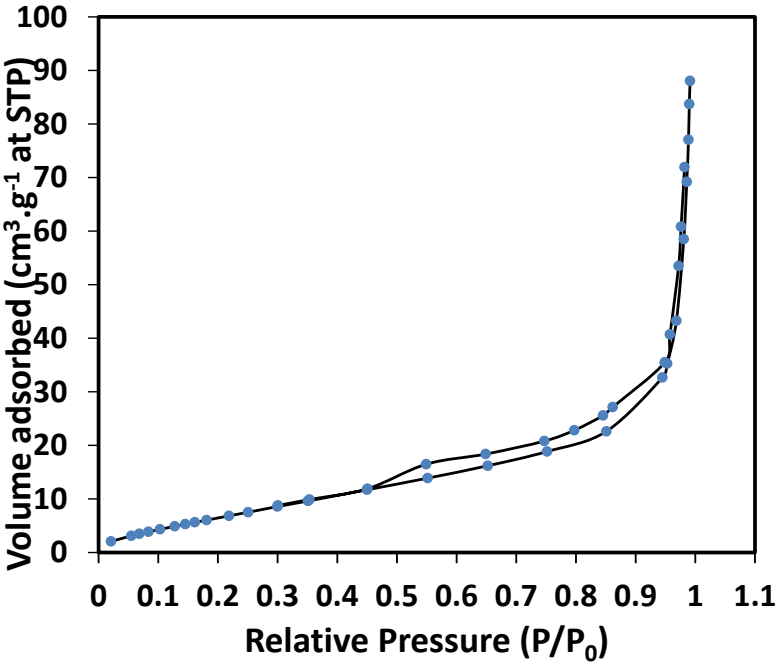

Fig. 5. N_2 adsorption-desorption of α-Fe_2O_3/MOF.

to form a flower-like structure.

The SEM image of α-Fe_2O_3/MOF was shown in Fig. (4-b_1). In this image, it is clear that α-Fe_2O_3 nanoparticles bind to MOF and occupy a large area of the porous and flower-like structure in MOF.

This image confirms that the α-Fe_2O_3 structures supported on the MOF is circular and elliptic tears and the size of these particles is less than 100 nm (about 70-90 nanometers). This particle size is consistent with the values obtained from X-ray diffraction patterns (the Debye-Scherrer calculation method). The α-Fe_2O_3 / MOF particle sizes distribution diagram (Fig. (4-b_1)) also confirms these particle sizes. The accumulation of Fe_2O_3 particles and their junction can be seen in the morphology of the sample obtained by transmission electron microscopy (Fig. 4-b_3).

Energy dispersive X-Ray (EDX) analysis has been used to identify the composition of the material. The EDX spectra of α-Fe_2O_3 /MOF (Fig. 4-c) confirms the presence of Fe and Cd in the sample. The presence of iron in the EDX analysis confirms the formation of iron oxide in the sample.

The N_2 adsorption-desorption isotherm of α-Fe_2O_3/MOF was shown in Fig. 5. The pore size distribution was determined by BJH analysis of the N_2 adsorption branch of this isotherm. Fig. 5 shows that α-Fe_2O_3/MOF isotherm is similar to standard type IV. At low relative pressure (less than 0.48) the adsorption was relatively small, while a more pronounced increase was observed in the higher relative pressure region (P/P_0 = 0.48-1.0). This could be a sign of pronounced capillary density in the mesoporous. A small residual ring in the range 0.45-1.0 at P/ P_0 was observed in the isotherm, which confirms the presence of low porous pores and narrow pores on the sample [18].

The Brunauer-Emmett-Teller (BET) method can show the value of the surface area of samples. Therefore, the BET surface area of the nano-flowers sample was determined by a nitrogen adsorption-desorption measurement. Surface area measurements reveal that Fe_2O_3/MOF has a BET surface area of 479 $m^2 g^{-1}$ and an average pore diameter of 112.5 nm.

Thermogravimetric analysis (TGA) was used to determine the thermal stability of the α-Fe_2O_3 / MOF (Fig.6). With increasing temperature, MOF and Fe_2O_3/MOF gradually lose weight. The loss of the guest molecule consisting of water adsorbed and the crystalline water of Fe_2O_3/ MOF was observed at 16 to 242 °C, and the loss of these guest molecules from the MOF was performed at 200 °C. The gradual collapse of the structure of MOF and Fe_2O_3/MOF has begun at 461°C and 512 °C respectively. These results indicate that

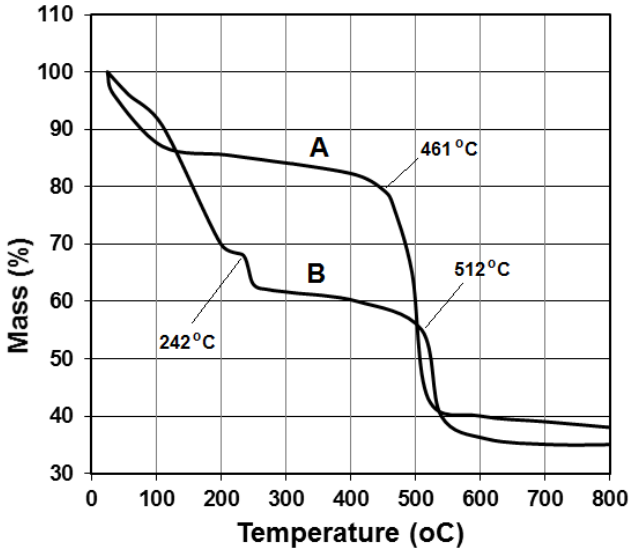

Fig. 6. TGA of MOF(A) and α-Fe_2O_3/MOF(B).

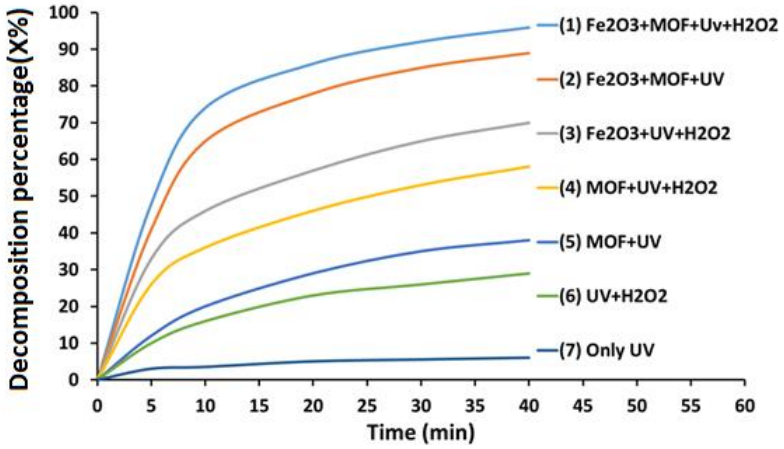

Fig. 7. Analyzing different modes of UV effects on CFX photocatalytic decomposition percentile (CFX initial concentration = 40 ppm, catalyst amount = 150 mg. l^{-1}, H_2O_2 initial concentration = 15 ppm, pH = 4).

the thermal stability of MOF was enhanced after α-Fe_2O_3 was loaded on the MOF structure or dispersed in the MOF pores.

Analysis of different modes of the effects of UV on CFX decomposition

Different methods of UV-C effect on CFX decomposition percentages are shown in Fig. 7. This Figure indicates that using UV-C, alone or with H_2O_2, has no significant effect on CFX photocatalytic decomposition; however, using some amounts of α-Fe_2O_3/MOF (50 mg. l^{-1}) increases decomposition percentages significantly. The highest decomposition of CFX has obtained from the simultaneous application of UV-C, H_2O_2, MOF and α-Fe_2O_3/MOF. The highest efficiency of decomposition occurs in the first 10 minutes of irradiation.

Factorial Design Modeling of the Tests

Evaluation of decomposition variables including α-Fe_2O_3/MOF amount, initial concentration of CFX, initial concentration H_2O_2 and pH is essential for optimizing photocatalytic processes. These factors are not independent, so the single-factor analysis will be a lengthy, incomplete, and complex process.

Table 3. Estimated coefficients and effects on CFX photocatalytic decomposition.

Term	Effect	Coefficient	T-Value	P-Value
Constant		69.3732	1781.28	0.000
Catalyst	10.4462	5.2231	123.07	0.000
CFX	-22.8113	-11.4056	-268.75	0.000
H_2O_2	4.5763	2.2881	53.91	0.000
pH	-5.6037	-2.8019	-66.02	0.000
Catalyst×CFX	-4.9087	-2.4544	-57.83	0.000
Catalyst×H_2O_2	6.8288	3.4144	80.45	0.000
Catalyst×pH	-4.3313	-2.1656	-51.03	0.000
CFX×H_2O_2	0.4263	0.2131	5.02	0.001
CFX×pH	-0.3087	-0.1544	-3.64	0.007
H_2O_2×pH	5.5287	2.7644	65.14	0.000

The use of statistical methods in the design of experiments such as the full factorial method can give a detailed analysis of the factors affecting the process. Saving time and requiring fewer trials to optimize the process are the advantages of this method. This method can also find the variable interactions.

Table 2 indicates CFX photocatalytic decomposition experiment design by the full factorial method. Decomposition percentage obtained with the equation (1):

$$\text{Decomposition percentile X \%} = \frac{A_0 - A_t}{A_0} \times 100 \quad (1)$$

Where A_0 and A_t are the absorbance value (in the λ_{max}=260nm) of the solution at 0 and t min, respectively.

The factorial design method was used based on Tables 1 and 2. In this method, all four variables were presented with the highest values (+1), median (0), and minimum values (-1). CFX photocatalytic decomposition percentage in the different condition are indicated in Table 2.

The effect of process variables on the response are given in Table 3. Positive numbers indicate that as the values of the variables increase, so does the response rate and vice versa. The results show that among the variables affecting the process, the initial concentration of CFX and pH has a negative effect on the response. The effects of the interaction of the variables are reported in Table 3. As shown in these results, the interaction of variables, namely the catalyst amount and the H_2O_2 initial concentration (Catalyst×H_2O_2) and CFX initial concentration and H_2O_2 initial concentration (CFX×H_2O_2) and also H_2O_2 initial concentration and pH (H_2O_2×pH) have positive effects. The other interactions of the variables were negative. It is important to note that P values have estimated with alpha (α) = 0.05.

Analysis of variance (ANOVA) is a type of statistical hypothesis test and this method based on a set of statistical models that are widely used in the analysis of experimental results [12,15]. In this research, ANOVA was applied to graphically analyze the experimental data to recognize the interaction between process variables and response. The accuracy of the polynomial model was determined according to the coefficient of determination R^2. Model terms were evaluated by the probability value(P-value) and the model quality was determined based on the statistical significance of the coefficients estimated by the Fisher Test (F-Value). The ANOVA results depicted in Table 4. In this Table, the number of parameters that can be changed in the process was shown with the DF column (degrees of freedom). Other columns show the adjusted sum of squares (Adj SS) and adjusted mean square (Adj MS). Standard deviation (S) is a dispersion index that represents the average data distance from the mean. In this study, the amount of standard deviation (0.16976) indicates a small dispersion from mean data. The determination coefficient (R-square) is a statistical measure that represents the ratio of the dependent variable's variance explained by variables in a regression model. The adjusted sum of squares (R-adjusted) quantifies the amount of variation in the response data that was explained by each term of the model. The determination coefficient always ranges from 0 to 1. Zero value means that the presented model explains none of the data changes around the mean, and 1 value indicates that the presented model explains all

Table 4. Variance analysis (ANOVA) of CFX photocatalytic decomposition.

Source	DF	Adj SS	Adj MS	F-Value	P-Value
Model	10	3208.61	320.86	11133.86	0.000
Linear	4	2727.29	681.82	23659.15	0.000
Catalyst	1	436.50	436.50	15146.40	0.000
CFX	1	2081.41	2081.41	72224.86	0.000
H_2O_2	1	83.77	83.77	2906.75	0.000
pH	1	125.61	125.61	4358.59	0.000
2-Way Interactions	6	481.33	80.22	2783.66	0.000
Catalyst × CFX	1	96.38	96.38	3344.49	0.000
Catalyst ×H_2O_2	1	186.53	186.53	6472.48	0.000
Catalyst ×pH	1	75.04	75.04	2603.84	0.000
CFX×H_2O_2	1	0.73	0.73	25.22	0.001
CFX×pH	1	0.38	0.38	13.23	0.007
H_2O_2×pH	1	122.27	0.03	4242.70	0.000
Error	8	0.23	0.03		
Lack-of-Fit	6	0.20	0.03	1.83	0.394
Pure Error	2	0.04	0.02		
Total	18	3208.84			

R^2 = 99.99%, R^2 (adj) = 99.98%, R^2 (pred) = 99.94%

the data changes around the mean. Therefore, the bigger R^2 is better [12]. In this study, determination, adjusted and predicted coefficients percentage for CFX photocatalytic decomposition in aqueous solution was obtained 99.99%, 99.98% and 99.94%, respectively, so it can be concluded that the proposed model is efficient for predicting the process.

The residual analysis of factorial design modeling for CFX photocatalytic decomposition in aqueous solution was illustrated in Fig. 8. In the normal probability diagram of the dispersion processes (Fig. 8 (a)), the points around the diagonal straight line represent the natural distribution of residual values or errors that require analysis of variance. In Fig. 8(b), there are two points that are almost on the zero lines, eight points in the below and seven points above the zero lines, which shows the random distribution of residual values (without specific rule) and confirm their independence. If the regression line crosses all the points of interactive data, all the changes can be explained. As the line gets away from the points, the data cannot be explained [15]. Repeatability and occurrence rates were represented in Fig. 8(c). If the F-Value of an experimental parameter was greater than the theoretical value, or the P-Value was less than 0.05, this parameter could affect results above 95%. The residual plots of each experiment were shown in Fig.8(d).

Pareto analysis allows you to eliminate unimportant factors in a process to focus your efforts on the factors that are most important. The Pareto chart (Fig. 9) was used to compare the standard effects of different variables in the modeling process, the analysis of the main variables and their interactions effects on the CFX decomposition photocatalytic process. As can be seen in Fig. 1, there are basically only two effects which are statistically important for photocatalytic decomposition of CFX, namely, in decreasing order of significance: the initial concentration of CFX and the catalyst amount. These effects are the most important factors affecting the photocatalytic decomposition of CFX. The catalyst amount significant effect is positive indicating that an increase in their level brings about an increase in the amount of CFX decomposed. The CFX initial concentration and H_2O_2 initial concentration (CFX×H_2O_2) as well as CFX initial concentration and pH (CFX×pH) in two-factor interactions are not very significant and may be explained as random noise.

In Fig. 10, the plots of the main effects have been shown. By ignoring the interactions, it can be deduced that the initial concentration of CFX has the most influence on the decomposition process. The decomposition percent was much increased

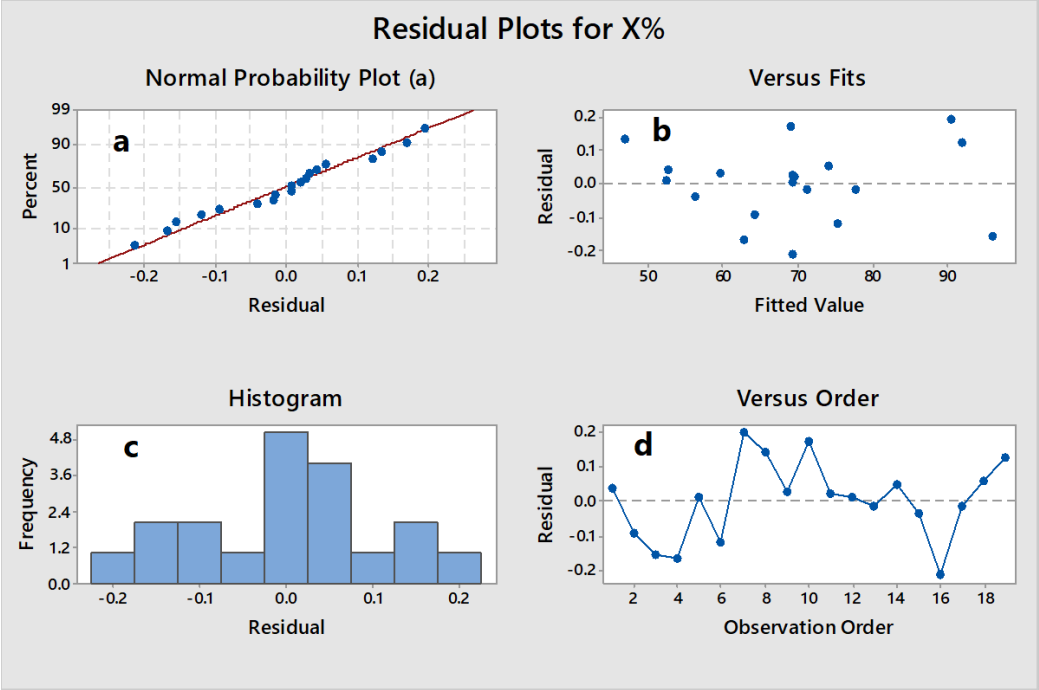

Fig. 8. Residual plots for CFX photocatalytic decomposition percentiles, (a) normal probability plot, (b) residual distribution dispersion coefficient versus efficient values, (c) repeatability and occurrence rate, (d) residual plots of each test.

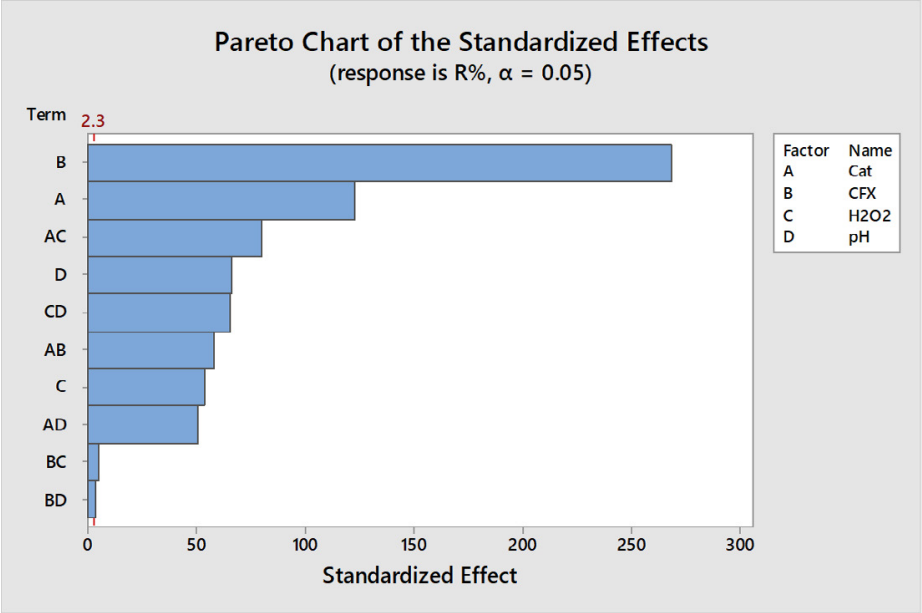

Fig. 9. Pareto Chart of standardization effects for photocatalytic decomposition of CFX.

with an increasing α-Fe_2O_3/MOF amount. With the increase of α-Fe_2O_3/MOF photocatalysts, OH radical production increases. pH and H_2O_2 concentration are the next levels of influence on the photocatalytic decomposition of CFX. If the pH increase, decomposition will decrease. The addition of hydrogen peroxide to the mixture in photocatalytic processes often results in increased

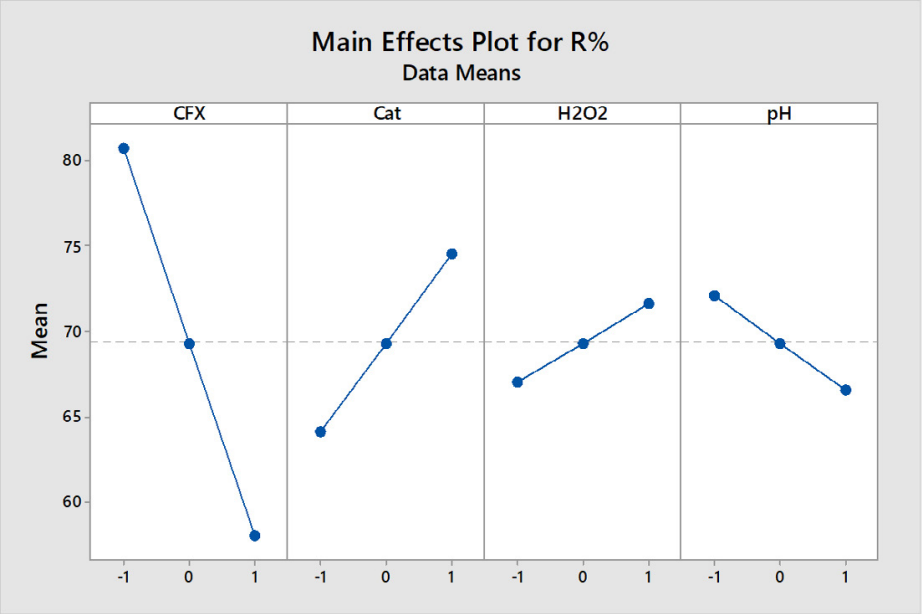

Fig. 10. Analyzing the effects of main variables on CFX photocatalytic decomposition percentiles.

decomposition of the pollutants. Other researchers conducted similar studies and concluding that H_2O_2 has a significant role in antibiotic oxidation [2]. In other words, H_2O_2 is an important agent of advanced oxidation and has a great influence on the rate of chemical reactions. Photolysis of hydrogen peroxide as a strong oxidant increases the efficiency of decomposition processes due to the production of hydroxide radicals. the concentration of H_2O_2 should be selected in accordance with the type and concentration of the pollutant. In the following reaction, hydrogen peroxide produces a hydroxide radical by adsorbing an electron from the semiconductor band (Reaction 6) [2].

$$H_2O_2 + e^- \rightarrow OH^\circ + OH^- \quad (6)$$

The pH of the solution effects on the adsorption capacity, the decomposition of the targeted compound, the electric charge distribution on photocatalyst surface, and the oxidation potential of the band [4]. The increased efficiency of this process in the acidic pH can be explained by the following (reactions 7-10), [13,19].

$$e^- + O_2 \rightarrow O_2^{\circ -} \quad (7)$$

$$O_2^{\circ -} + H^+ \rightarrow HO_2^\circ \quad (8)$$

$$2HO_2^\circ \rightarrow O_2 + H_2O_2 \quad (9)$$

$$H_2O_2 + O_2^{\circ -} \rightarrow OH^\circ + OH^- + O_2 \quad (10)$$

The statistical model of sample data was evaluated by a regression analysis method. The mathematical model is as the equation (2):

X%=69.3732+ 5.2231 A- 11.4056 B+ 2.2881 C- 2.8019 D- 2.4544 AB+3.4144 AC
-2.1656 AD+ 0.2131 BC - 0.1544 BD + 2.7644 CD (2)

wherein A, B, C, D are α-Fe_2O_3/MOF amounts, initial concentration of CFX, initial concentration of H_2O_2, and pH value respectively.

Kinetic of Photocatalytic Decomposition of CFX

The ln(A_0/A) was plotted versus reaction time for CFX photocatalytic decomposition in the optimum condition (Fig. 11). The linearity of this graph indicates that the reaction kinetic is pseudo-first-order [19-21]. The rate coefficient of this reaction was determined according to the slope of the line (k=0.0769 min^{-1}).

In order to reuse the photocatalyst, the experiment was repeated in the optimum condition for five times. The results of removal

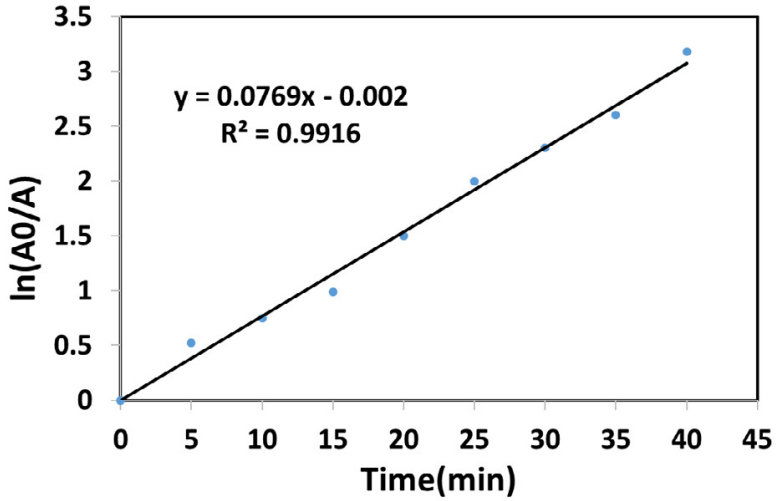

Fig. 11. Kinetic plot of ln (A_0/A) versus irradiation time for CFX photocatalytic decomposition (CFX concentration = 40 ppm, α-Fe_2O_3/MOF amount= 150 mg. L^{-1}, H_2O_2 concentration= 15 ppm, pH = 4).

Table 5. Previous research on the elimination of Cefalexin by photocatalytic method.

Photocatalyst	Condition	Degradation efficiency	References
CdSe quantum dots (QDs)	0.5 g.l^{-1} catalyst and 100 mL of 15 mg.l^{-1} aqueous solution of antibiotic wastewater, irradiating with a 300 W model GGZ300 UV high pressure mercury lamp (365 nm).	70.34% after 60 min	[22]
MgO/granular activated carbon (GAC) composite	Initial concentration of cefalexin was 20 mg.l^{-1}, pH=3 and 4 g.l^{-1} of MgO/GAC composite with UV irradiation.	98% after 60 min	[23]
PbS-CdS-Clinoptilolite (CP)	Optimal experimental parameters (1.5 g.l^{-1} of the photocatalyst, 25mg.l^{-1} solution at pH 3.0 and 2 UV tubes each of 35 W)	92% (TOC removal)after 360 min	[24]
ZnO nanowires	100 µg.l^{-1} cephalexin, 80 mg.l^{-1} ZnO nanowires, pH=7.2, air-cooled 1700W Xenon lamp	100% after 45 min	[25]
g-C_3N_4@ZnO	10 mg.l^{-1} cephalexin and 0.3 g.l^{-1} photocatalyst, Xenon lamp (300 W)	98.9% after 60 min	[26]

efficiency (X_1=95.84%, X_2=95.82%, X_3=95.81%, X_4=95.78% and X_5=95.75%) confirm reuse capability of α-Fe_2O_3 /MOF photocatalyst.

To confirm the cefalexin mineralization in the photocatalytic process, the amount of total organic carbon (TOC) and the chemical oxygen demands (COD) was measured under optimum condition. To confirm the cefalexin mineralization in the photocatalytic process, the amount of total organic carbon (TOC) and the chemical oxygen demands (COD) was measured under optimum conditions. The results shown that 71% TOC and 80.2% COD were decreased after 60 min of irradiation.

The most important previous researches on cephalexin removal by photocatalytic methods were summarized in Table 5. Due to the different conditions of the process in these studies, it is difficult to compare their results with each other. According to the results, the greatest percentage of cefalexin removal was obtained using ZnO nanowire photo-catalyst. It should be noted that the concentration of cephalexin has been little (100 µg. l^{-1}) in this procedure and the energy consumption (1700 watts) has been higher than all other processes [25].

The usage of graphitic carbon nitrides (g-C_3N_4) @ZnO catalyst has given similar results with ZnO nanowires in the photocatalytic elimination of cefalexin. The (g-C_3N_4) @ZnO shown a great percentage of removal (about 98.9 after 60 min%). Due to the high cost of the catalyst and high energy consumption, the use of this catalyst is not cost-effective. [26].

Although the use of MgO / GAC catalysts has resulted in a higher removal percentage compared

to the α-Fe_2O_3 /MOF catalyst (was used in this study), the amount of catalyst and irradiation time in the process have been high [23].

According to the explanations provided in this paper, the preparation of α-Fe_2O_3 /MOF photo-catalyst is relatively simple and inexpensive and has high stability in aqueous solution. Also, it has a good degradation efficiency (95.84% after 40 min) in the photocatalytic decomposition of cefalexin aqueous solution.

CONCLUSION

The results showed that the metal-organic framework could be synthesized using cadmium nitrate and terephthalic acid. The structure of this framework was confirmed by XRD, FTIR and EXD experiments, and their morphology can be identified by SEM and TEM images. High surface areas, regular pores and cluster structure of MOF make it a suitable base for α-Fe_2O_3 nano-photocatalyst. The α-Fe_2O_3 nanoparticles (supported on the MOF) are interconnected and occupy more surface area on the crystalline surfaces of MOF, which enhances the efficiency of the photocatalytic decomposition processes. The SSD is a suitable method for supporting of α-Fe_2O_3 on the MOF. Statistical analysis of the results confirmed the reliability and validity of this model. If the variables do not interact, the initial concentration of H_2O_2 and α-Fe_2O_3 / MOF will have positive effects and the initial concentration of CFX and pH will have negative effects on CFX decomposition. The variables interaction is very important to optimize the decomposition process. Finally, we recommend using this catalyst for removing of other organic pollutants in the water by photocatalytic method.

ACKNOWLEDGMENT

The authors express their gratitude to the Islamic Azad University of Arak for supporting the laboratory equipment.

CONFLICT OF INTEREST

Authors have no conflict of interest.

REFERENCES

1. Gualerzi C. O., Brandi L., Fabbretti A., Pon C. I., (2013), Antibiotics: Targets, Mechanisms and Resistance. *Weinheim*, Germany: Wiley-VCH.
2. Yuan F., Hu C., Hu X., Qu J., Yang M., (2009), Degradation of selected pharmaceuticals in aqueous solution with UV and UV/H_2O_2. *Water Res.* 43: 1766–1774.
3. Balcioglu I. A., Otker M., (2003), Treatment of pharmaceutical wastewater containing antibiotics by O_3 and O_3/H_2O_2 processes. *Chemosphere.* 50: 85–95.
4. Jung Y., Gikim W., Yoon Y., Kang J. W., Hong Y. M., Kim H. W., (2012), Removal of amoxicillin by UV and UV/H_2O_2 processes. *Sci. Total Environ.* 420: 160–167.
5. Jiao S., Zheng S., Yin D., Wang L., Chen L., (2008), Aqueous photolysis of tetracycline and toxicity of photocatalytic products to luminescent bacteria. *Chemosphere.* 73: 377–382.
6. Muhajir M., Puspitasari P., Razak J. A., (2019), Synthesis and applications of Hematite α-Fe_2O_3: A Review. *J. Mech. Eng. Sci. Technol.* 3: 51-58.
7. Mishra M., Chun D. M., (2015), α-Fe_2O_3 as a photocatalytic material: A review. *Appl. Catal. A*. 498: 126–141.
8. Safaei M., Foroughi M. M., Ebrahimpoor N., Jahani S., Omidi A., Khatami M., (2019), A review on metal-organic frameworks: Synthesis and applications. *Trends Anal. Chem.* 118: 401-425.
9. Rowsel J. L. C., Yaghi O. M., (2004), Metal–organic frameworks: a new class of porous materials. *Microporous Mesoporous Mater*. 73: 3–14.
10. Kaskel S., (2016), The Chemistry of Metal-Organic Frameworks: Synthesis, Characterization, and Applications. *Weinheim,* Germany: Wiley-VCH.
11. Bharathi S., Nataraj D., Mangalaraj D., Masuda Y., Senthil K., Yong K., (2010), Highly mesoporous α–Fe_2O_3 nanostructures: Preparation, characterization and improved photocatalytic performance towards Rhodamine B (RhB). *J. Phys. D: Appl. Phys*. 43: 1–9.
12. Sakkas V. A., Islam M. A., Stalikas C., Albanis T. A., (2010), Photocatalytic degradation using design of experiments: A review and example of the Congo red degradation. *J. Hazard. Mater*. 175: 33-44.
13. Saghi M., Mahanpoor K., Shafiei H., (2018), Preparation of nano spherical α-Fe_2O_3 supported on 12- Tungestosilicilic acid using two different methods: A novel catalyst. *Iran. J. Chem. Chem. Eng.* 37:1–10.
14. Jafari M., Salehi M., Behzad M., (2018), Structural, magnetic and electrical properties of pure and Dy-doped Fe_2O_3 nanostructures synthesized using chemical thermal decomposition technique. *Int. J. Nano Dimens*. 9: 179-190.
15. Saghi M., Mahanpoor K., (2017), Photocatalytic degradation of tetracycline aqueous solutions by nanospherical α-Fe_2O_3 supported on 12-Tangesilicilic acid as catalyst: Using full factorial experimental design. *Int. J. Ind. Chem*. 8: 297-313.
16. Malecka B., Lacz A., (2008), Thermal deposition of cadmium format in inert and oxidative atmosphere. *Thermochim. Acta*. 479: 12-16.
17. Hargreaves J. S. J., (2016), Some considerations related to the use of the Scherrer equation in powder X-ray diffraction as applied to heterogeneous catalysts. *Catal. Struct. React*. 2: 33-37
18. Sheibani N., Kazemipour M., Jahani S., Foroughi M. M., (2019), A novel highly sensitive thebaine sensor based on MWCNT and dandelion-like Co_3O_4 nanoflowers fabricated via solvothermal synthesis. *Microchem. J.* 149: 103980-103986.
19. Elmolla E. S., Chaudhuri M., (2010), Photocatalytic degradation of amoxicillin, ampicillin and cloxacillin antibiotics in aqueous solution using UV/TiO_2 and UV/H_2O_2/TiO_2 photo catalysis. *Desalination*. 252: 46–52.
20. French R. A., Jacobson A. R., Kim B., Isley S. L., Penn R. L.,

Baveye P. C., (2009), Influence of ionic strength, pH and cation valence on aggregation kinetics of titanium dioxide nanoparticles. *Environ Sci., Technol*. 43: 1354–1359.
21. Foroughi M. M., Jahani S., Rajaei M., (2019), Facile fabrication of 3D Dandelion-like cobalt oxide Nanoflowers and its functionalization in the first electrochemical sensing of oxymorphone: Evaluation of kinetic parameters at the surface electrode. *J. Electrochem. Soc*. 166: B1300–B1311.
22. Liu X., Ma C., Yan Y., Yao G., Tang Y., Huo P., Shi W., Yan Y., (2013), Hydrothermal synthesis of CdSe quantum dots and their photocatalytic activity on degradation of cephalexin. *Ind. Eng. Chem. Res*. 52: 15015−15023.
23. Seid-Mohammadi A., Bahrami M., Omari S., Asadi F., (2019), Removal of cephalexin from aqueous solutions using magnesium oxide/granular activated carbon hybrid photocatalytic process. *Avic. J. Environ. Health Eng*. 6: 24-32.
24. Azimi S., Nezamzadeh-Ejhieh A., (2015), Enhanced activity of clinoptilolite-supported hybridized PbS-CdS semiconductors for the photocatalytic degradation of a mixture of tetracycline and cephalexin aqueous solution. *J. Mol. Catal. A: Chem*. 408: 152-160.
25. Hea J., Zhang Y., Guo Y., Rhodes G., Yeom J., Lia H., Zhang W., (2019), Photocatalytic degradation of cephalexin by ZnO nanowires under simulated sunlight: Kinetics, influencing factors, and mechanisms. *Environ. Int*. 132: 1-10.
26. Li N., Tian Y., Zhao J., Zhang J., Zuo W., Kong L., Cui H., (2018), Z-scheme 2D/3D g-C_3N_4@ZnO with enhanced photocatalytic activity for cephalexin oxidation under solar light. *Chem. Eng. J*. 352: 412-422.